

A Primer on Large Intelligent Surface (LIS) for Wireless Sensing in an Industrial Setting

Cristian J. Vaca-Rubio*, Pablo Ramirez-Espinosa*, Robin Jess Williams*, Kimmo Kansanen[†],
Zheng-Hua Tan[‡], Elisabeth de Carvalho* and Petar Popovski*

*Department of Electronic Systems, Connectivity Section (CNT) Aalborg University, Denmark

[†]Norwegian University of Science and Technology, Trondheim, Norway

[‡]Department of Electronic Systems, Signal and Information Processing Section (SIP) Aalborg University, Denmark
email: {civr, pres, rjw}@es.aau.dk, kimmo.kansanen@ntnu.no, {zt, edc, petarp}@es.aau.dk

Abstract—One of the beyond-5G developments that is often highlighted is the integration of wireless communication and radio sensing. This paper addresses the potential of communication-sensing integration of Large Intelligent Surfaces (LIS) in an exemplary Industry 4.0 scenario. Besides the potential for high throughput and efficient multiplexing of wireless links, a LIS can offer a high-resolution rendering of the propagation environment. This is because, in an indoor setting, it can be placed in proximity to the sensed phenomena, while the high resolution is offered by densely spaced tiny antennas deployed over a large area. By treating a LIS as a radio image of the environment, we develop sensing techniques that leverage the tools of image processing and computer vision combined with machine learning. We test these methods for a scenario where we need to detect whether an industrial robot deviates from a predefined route. The results show that the LIS-based sensing offers high precision and has a high application potential in indoor industrial environments.

I. INTRODUCTION

Massive multiple-input multiple-output (MIMO) is a fundamental technology in the 5th generation of wireless networks (5G), with the addition of a large number of antennas per base station as its key feature [1]. Looking towards post-5G, researchers are defining a new generation of base stations that are equipped with an even larger number of antennas, giving rise to the concept of large intelligent surface (LIS). Formally, a LIS designates a large continuous electromagnetic surface able to transmit and receive radio waves [2], which can be easily integrated into the propagation environment, e.g., placed on walls. In practice, a LIS is composed of a collection of closely spaced tiny antenna elements. Whilst the performance of LIS in communications has received considerably attention recently [3]–[5], the potential of these devices could go beyond communications applications, e.g., environment sensing. Indeed, such large surfaces contain many antennas that can be used as sensors of the environment based on the channel state information (CSI).

Sensing strategies have been widely addressed in the literature in different ways, being the measured magnitude the main

distinction between them. Thus, we can find sensing methods based on the communication signals produced by active users [6], Doppler shifts [7], radio tomographic images obtained from the received signal strength [8], [9] or radar-like sensing [10], [11], to mention but a few of relevant examples. Interestingly, whilst some of these sensing techniques resort solely on the amplitude — equivalently, power — of the receive signals [8], [9], in those cases where sensing small scale variations is needed, the full CSI —i.e., amplitude and phase of the impinging signals — is required [10], [11].

On a related note, machine learning (ML) based approaches are gaining popularity in the context of massive MIMO systems, providing suitable solutions to optimization problems [12], [13]. Due to the large dimensions of the system in extra-large arrays, it is crucial to use deep learning to exploit complex patterns of information dependency between the transmitted signals. The popularization of LIS as a natural next step from massive MIMO gives rise to larger arrays and more degrees of freedom, providing huge amounts of data which can feed ML algorithms. Hence, deep learning arises as a potential solution to exploit the performance of LIS.

In this work, we aim to pave the way to the combined use of both deep learning algorithms and the aforementioned large surfaces, exploring, for first time in the literature, the potential of such a joint solution to sense the propagation environment. Specifically, the contribution of this work is twofold:

- We propose an image-based sensing technique based on the received signal power at each antenna element of a LIS. These power samples are processed to generate an high resolution image of the propagation environment that can be used to feed computer vision algorithms to sense large-scale events.
- A computer vision algorithm, based on transfer learning and support vector machine (SVM), is defined to process the radio images generated by the LIS in order to detect anomalies over a predefined robot route.

The performance of the proposed solution is tested in an indoor industrial scenario, where the impact of the array aperture and the inter-antenna distance is thoroughly evaluated. We show that both larger apertures and smaller separations

This project has received funding from the European Union's Horizon 2020 research and innovation programme under the Marie Skłodowska-Curie grant agreement No 813999.

This work has been submitted to the IEEE for possible publication. Copyright may be transferred without notice, after which this version may no longer be accessible.

between the LIS elements render higher resolution images, improving the performance of the system.

II. PROBLEM FORMULATION

We consider an industrial scenario where a robot is supposed to follow a fixed route, and assume that, due to arbitrary reasons, it might deviate from the predefined route and follow an alternative (undesired) trajectory. Hence, our goal is, based on the sensing signal transmitted by the target device, being able to detect whether the robot is following the correct route or not.

In order to perform the anomalous route detection, we assume that a LIS (i.e., a large array of closely spaced antennas), is placed in the scenario. Therefore, the sensing problem reduces to determine, from the received signal at each of the LIS elements, if the transmission has been made from a point at the desired route or from anomalous ones. Due to the fact that, in general, acquiring an accurate CSI is a non-trivial task, we resort on the received signal amplitude (equivalently, power), which may lead to simpler systems implementations. To understand the necessity of large arrays and ML techniques to tackle this problem, let consider the following preliminary example:

Assume that we have two points, p_1 and p_2 , belonging to the desired and the anomalous route, respectively. Then, the received complex signal vector at the array of M antennas from p_1 and p_2 is given by

$$\mathbf{y}_k = \mathbf{h}_k + \mathbf{n}_k, \quad k = 1, 2, \quad (1)$$

where \mathbf{h}_k is the complex noiseless received signal (channel) and $\mathbf{n}_k \sim \mathcal{CN}_M(\mathbf{0}, \sigma^2 \mathbf{I})$ represents the noise vector. To verify that p_1 and p_2 are actually points belonging to different trajectories, we could try to perform an hypothesis testing based on the euclidean distance between the received signal amplitudes, i.e.,

$$\frac{1}{M} \|\mathbf{y}_1 - \mathbf{y}_2\|^2 = \frac{1}{M} \sum_{i=1}^M |y_{1,i}|^2 + |y_{2,i}|^2 - 2\text{Re}\{|y_{1,i}| |y_{2,i}|\}, \quad (2)$$

with $y_{k,i}$ denoting the elements of \mathbf{y}_k . If we consider that M is sufficiently large, then the law of large numbers holds and (2) is rewritten as

$$\begin{aligned} \frac{1}{M} \|\mathbf{y}_1 - \mathbf{y}_2\|^2 &= \frac{1}{M} \sum_{i=1}^M [|h_{1,i}|^2 + |h_{2,i}|^2] \\ &\quad + 2\sigma^2 - \frac{2}{M^2} \sum_{i=1}^M |y_{1,i}| \sum_{i=1}^M |y_{2,i}|. \end{aligned} \quad (3)$$

In (3), the first term is the sum of the average power of the channels, whilst the second term represents the equivalent noise, which completely depends on the channel realizations. If we would perform an hypothesis testing in order to establish a certain threshold that determines if the two points are in different routes, then the variance of the error term would determine the probability of failure. Note that, to obtain an optimum estimator, we would need to know all the possible states of the channels for each path. Moreover, even in the most simple case, i.e., assuming a pure line-of-sight (LoS)

propagation, we would still be unable to distinguish if the two points are in different trajectories or at distinct positions of the same route.

The use of a very large number of antennas arises as a possible solution to mitigate the effect of the noise term. For the sake of illustration, Fig. 2 depicts the variance of the noise term as a function of the number of antenna elements in a pure LoS propagation environment, showing clearly how the variance tends to zero as the number of antennas increases.

However, although the use of a large number of elements in the LIS may reduce the noise variance, in a realistic environment, the complexity of the propagation paths is considerable, and the theoretical analysis becomes cumbersome and site-dependent. Hence, in order to gain insight into how the propagation paths between different positions translate into differences in the received signals, we have to resort on machine learning algorithms. This, together with the use of LIS, can provide the necessary information about the propagation environment in order to perform the anomalous route detection.

III. HOLOGRAPHIC SENSING

A hologram is a recorded interference pattern as a result of constructive and destructive combinations of the superimposed light-wavefronts, i.e., a photographic recording of a light field [14]. In a wireless context, a LIS could be described as a structure which uses electromagnetic signals impinging in a determined scatterer in order to obtain a profile of the environment. That is, we can use the received signal power received at each of the multiple elements of the LIS to obtain a high resolution image of the propagation environment. Using this approach, the complexity of the multipath propagation is reduced to using information represented as an image. This provides a twofold benefit: *i*) the massive number of elements that composed the LIS leads to an accurate environment sensing, and *ii*) it allows the use of computer vision algorithms and image processing techniques to deal with the resulting images.

As an illustrative example, Fig. 1 shows the holographic images obtained from different propagation environments. Specifically, Figs. 1a and 1b correspond to a LoS propagation (no scatterers), whilst Figs. 1c and 1d were obtained from an industrial scenario with a rich scattering. Note that, in the case in which different scatterers are placed, their position and shapes are captured by the LIS and represented in the image. Thanks to the large aperture offered by the surface, we are able to reconstruct a feature map (image) that describes what is occurring in space, based on the information acquired from the radio propagation environment. To the best of the authors' knowledge, this is the first time that imaged-based sensing is proposed in the literature.

IV. MACHINE LEARNING FOR HOLOGRAPHIC SENSING

A. Model description

We here propose the use of a machine learning model to perform the anomalous route classification task, based on the holographic images obtained at the LIS. In our considered problem, the training data is obtained by measuring the received

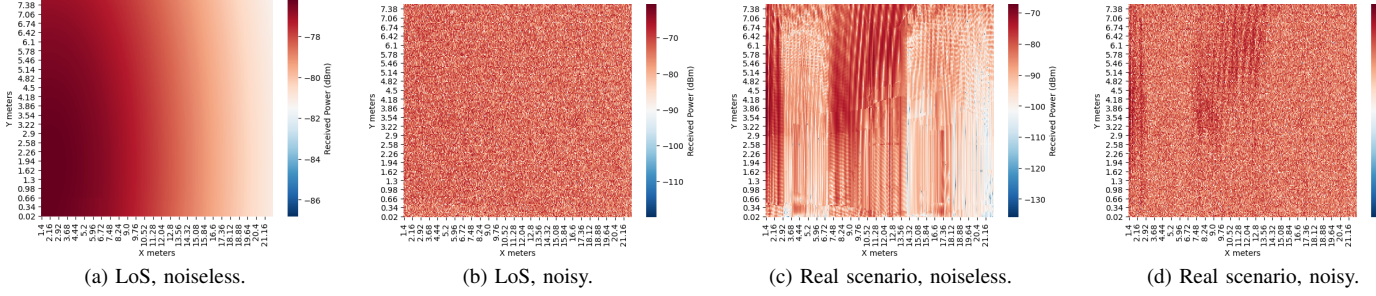


Fig. 1. Holographic images for LoS and Industry scenarios. The noisy holographic images are shown for a SNR of $\gamma = -40$ dB.

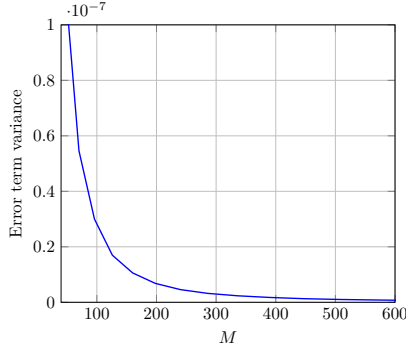


Fig. 2. Equivalent noise term variance in terms of M in a LoS scenario.

power at certain temporal instants while the target device is moving along the route. Therefore, the amount of data available depends on the length of the route and the sampling period, which may lead in some cases to an insufficient dataset to completely train the model. A solution to this issue is making use of transfer learning [15]. Among the available strategies for this matter, we will use feature representation.

One of the main requirements for transfer learning is the presence of models that perform well on already defined tasks. These models are usually shared in the form of a large number of parameters/weights the model achieved while being trained to a stable state [16]. The famous deep learning Python library, Keras [17], provides an easy way to reuse some of this popular models. Due to our large number of features (the RGB values of each pixel in the holographic image), and the training data constraints, we propose the use of a SVM binary classifier, which has been proved to perform correctly in the aforementioned conditions [18].

The model is detailed in Fig. 3, and consists in two clearly differentiated parts: *i*) feature extractor by using VGG19, and *ii*) SVM binary classifier. The first diagram corresponds to the original VGG19 architecture. In order to perform the feature extraction, we remove the last fully connected layer (FC) that performs the classification for the purpose of VGG19 and modify it for our specific classification task (anomaly/not anomaly in robot's route). We note that the architecture has been frozen for our case, i.e., the weights and biases in VGG19 are not re-trained along the process. Instead, they are re-used to generate the features that will be later used to feed the SVM

binary classifier. Hence, only the SVM will be trained by using the extracted features.

B. Dataset format

The dataset is obtained by sampling the received signal power at each element of the LIS while the robot moves along the trajectory, containing then T samples (holographic image snapshots of received power). At each sample, the input is an image represented by a matrix with $n_c = 3$ channels (RGB) of size $n_w = 224$ and $n_h = 224$ pixels. Our data can then be denoted as $\{X^{(i)}, y^{(i)}\}_{i=1}^T$, where $X^{(i)}$ is the i -th $n_w \times n_h$ input features matrix and $y^{(i)}$ is the corresponding desired output label associated to the image (anomaly or not anomaly).

Once the feature extraction is performed, the output is $n_c = 512$ channels of size $n_w = 7$ and $n_h = 7$ pixels. Since SVM works with vectors, the data is reshaped into an input feature vector formed by $7 \times 7 \times 512 = 25088$ features, being now our data $\{x^{(i)}, y^{(i)}\}_{i=1}^T$, where $x^{(i)}$ is the i -th n -dimensional training input features vector (being $n = 25088$), $x_j^{(i)}$ is the value of the j -th feature, and $y^{(i)}$ is the corresponding desired output label vector.

V. MODEL VALIDATION

In order to validate the proposed method, we carried out an extensive set of simulations to analyze the performance of the classification algorithm based on holographic images. To properly obtain the received power values, we make use of a ray tracing software, so we can capture the effects of the multipath propagation in the most reliable way. Specifically, we consider ALTAIR FEKO WINPROP [19].

A. Simulated scenario

The baseline set-up is described in Fig. 4a. A typical small size industrial scenario of size 484 m^2 , where the target robot (highlighted in red colour) follows a horizontal fixed route parallel to the bottom wall, in which the LIS is deployed. The distance between the LIS and the desired trajectory is 13.9 m , and three anomalous routes are considered, with a separation of 0.5 m within them, as detailed in Fig. 4b.

For these routes, we simulate in the ray tracing software T time steps, which corresponds to different positions of the robot in both the correct and anomalous routes. Then, a holographic

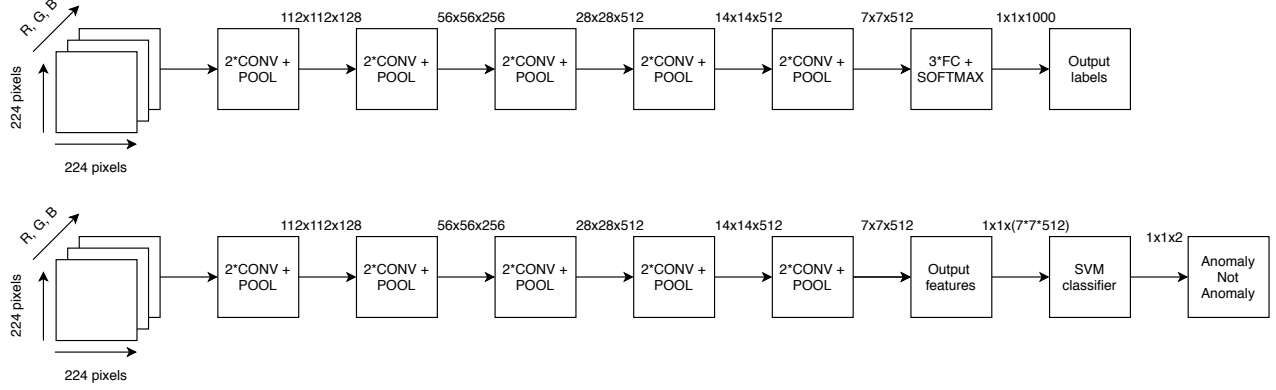


Fig. 3. VGG19 and proposed feature extractors.

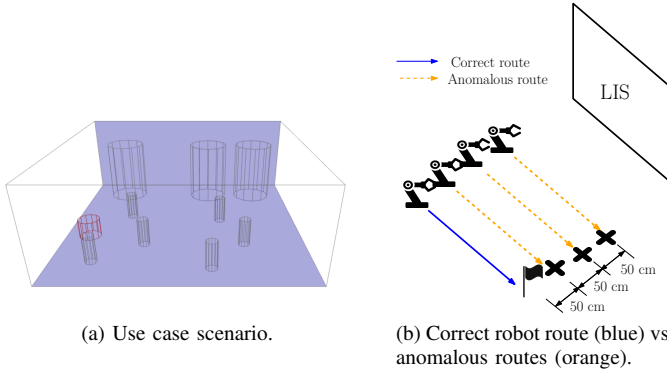


Fig. 4. Simulated scenario.

image snapshot of the measurements is taken at every T . The most relevant parameters used for simulation are summarized in Table I.

TABLE I. PARAMETERS

Frequency (GHz)	Tx Power (dBm)	Nray paths	Antenna type	Surface width dimension (m)	Surface height dimension (m)	Antenna Spacing (cm)	Propagation model
3.5	20	20	Omni	22	8	$\frac{\lambda}{2}/\lambda/2\lambda$	Free Space

In our simulations, we set $T = 365$, and thus the dataset is composed of 365 radio propagation snapshots containing images of anomaly and not anomaly situations, as described in Section IV-B. The dataset is then split into a 80% training set and 20% for the test set. During the training phase, the hyperparameter C is tuned to prevent overfitting by controlling the balance between bias and variance in the SVM model. The optimum value used is $C = 0.001$, which was identified by using a 5-fold cross-validation strategy [20].

B. Received power and noise modeling

The complex electric field arriving at the i -th antenna element at sample time t , $\tilde{E}_i(t)$, can be regarded as the su-

perposition of each path, i.e.,

$$\tilde{E}_i(t) = \sum_{n=1}^{N_r} \tilde{E}_{i,n}(t) = \sum_{n=1}^{N_r} E_{i,n}(t) e^{j\phi_{i,n}(t)}, \quad (4)$$

where N_r is the number of paths and $\tilde{E}_{i,n}(t)$ is the complex electric field at i -th antenna from n -th path, with amplitude $E_{i,n}(t)$ and phase $\phi_{i,n}(t)$. From (4), and assuming isotropic antennas, the complex signal at the output of the i -th element is therefore given by

$$\tilde{V}_i(t) = \sqrt{\frac{\lambda^2 Z_i}{4\pi Z_0}} \tilde{E}_i(t) + n_i(t), \quad (5)$$

with λ the wavelength, $Z_0 = 120\pi$ the free space impedance, Z_i the antenna impedance, and $n_i(t)$ is complex Gaussian noise with zero mean and variance σ^2 . For simplicity, we consider $Z_i = 1 \forall i$. Thus, the power $W_i(t) = |\tilde{V}_i(t)|^2$ is used at each temporal instant t to generate the holographic image. Finally, in order to test the system performance under distinct noise conditions, the average signal-to-noise ratio (SNR), γ , is defined as

$$\gamma \triangleq \frac{\lambda^2}{4\pi Z_0 M T \sigma^2} \sum_{t=1}^T \sum_{i=1}^M |\tilde{E}_i(t)|^2, \quad (6)$$

where M denotes the number of antenna elements in the LIS.

C. Performance metrics

To evaluate the prediction effectiveness of our proposed method, we resort on common performance metrics that are widely used in the related literature. Concretely, we are focusing on the F1-Score which is a metric based on the Precision and Recall metrics [21] and is described as:

- Positive F1-Score (PF_1) and Negative F1-Score (NF_1) as the harmonic mean of precision and recall:

$$PF_1 = 2 \cdot \frac{PP \cdot RP}{PP + RP}, \quad NF_1 = 2 \cdot \frac{PN \cdot RN}{PN + RN}. \quad (7)$$

Where PP and RP stand for Precision and Recall of the positive class (anomaly) while PN and RN stand for Precision and Recall of the negative class (not anomalous situation).

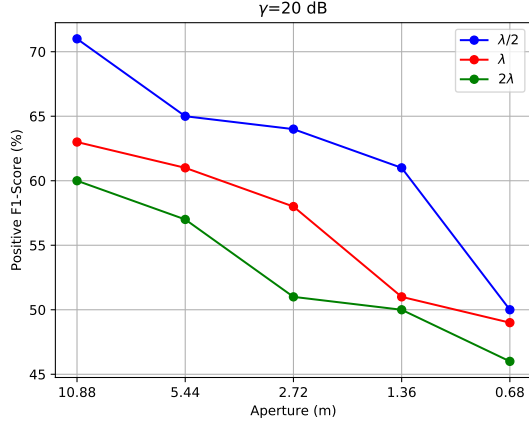


Fig. 5. PF_1 score in terms of the array aperture for distinct spaces.

VI. NUMERICAL RESULTS AND DISCUSSION

We now analyze the system performance in terms of the different involved parameters. Specifically, we focus on the impact of the array aperture, the distance between the distinct elements of the LIS, and the relation between them.

Generally, in the considered industrial setup, it would be more desirable to avoid undetected anomalies (which may indicate some error in the robot or some external issue in the predefined trajectory) than obtaining a false positive. Hence, all the figures in this section shows the algorithm performance in terms of the PF_1 metric. Nevertheless, for reader's convenience, the NF_1 metric is also provided in tables for all the cases under consideration.

A. Impact of spacing and aperture

To evaluate the impact of both spacing and aperture, we consider linear arrays, extracted at the middle height of the wall. We assume a fixed γ for all the cases ($\gamma = 20$ dB), and different spacings with respect to the wavelength ($\lambda/2$, λ and 2λ). Note that the majority of the variations of the pattern in the holographic images are contained in the horizontal axis, being of interest to analyze this information. The performance results for the distinct configurations are depicted in Fig. 5 and summarized in Table II. As observed, the spacing of 2λ — which is far from the concept of LIS — is presenting really inaccurate results showing that the resolution obtained for that spacing is quite poor. Hence, it is concluded that the quick variations along the surface provide important information to the classifier performance. Here, the effect of antenna densification for a given aperture is highlighted and it can be seen that the lowest spacing leads to the best results.

B. LIS and horizontal array comparison

To show the potential of LIS for sensing, a comparison between using the LIS (understanding by LIS the use of the whole wall) and several horizontal array configurations taken at middle height of the LIS (128, 64 and 8 antennas) are considered for the best spacing case ($\lambda/2$). The results are

TABLE II. RESULTS SUMMARY APERTURE VS SPACING

		Apertures (m)					
		10.88	5.44	2.72	1.36	0.68	
$\lambda/2$	PF_1 (%)	71	65	64	61	50	
	NF_1 (%)	71	69	62	57	50	
λ	PF_1 (%)	63	61	58	51	49	
	NF_1 (%)	37	66	51	50	46	
2λ	PF_1 (%)	60	57	51	50	46	
	NF_1 (%)	60	51	50	49	42	

plotted in Fig. 6 in terms of γ , and summarized in Table III. Overall, we observe that system performance is worsened as the noise is increased or the aperture is decreased, which are in fact expected results. Regarding Fig. 6, we not only observe that the use of a LIS leads to a considerable better performance, but also that it is more robust against noise. This is coherent with the massive MIMO effect highlighted in Section II, where the variance of the resulting noise term reduces as we increase the number of antennas. Moreover, the LIS system robustness to noise in the low $\gamma = -30$ dB scenario shows the potential of using a full holographic image which captures accurately the macroscopic pattern of the propagation environment based on low power sensing signals (which may be interesting for autonomous devices where energy efficiency is a desired requirement). As a final remark, it is clear that a bigger aperture and extra dimension (vertical axis of LIS) is adding insightful information of the sensed environment, something expected taking into account the impact of the aperture described previously.

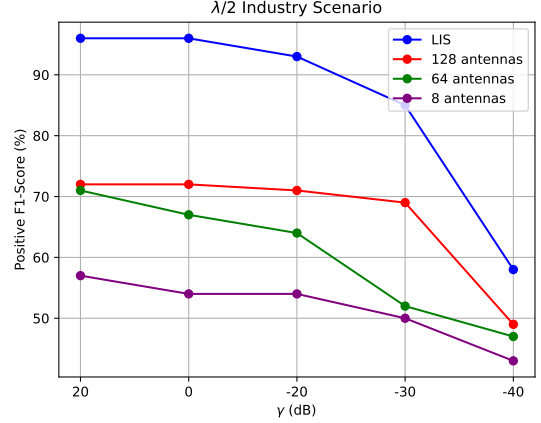


Fig. 6. PF_1 score in terms of γ for distinct array configurations.

TABLE III. RESULTS SUMMARY LIS VS ARRAY CONFIGURATIONS

		γ (dB)				
		20	0	-20	-30	-40
LIS	PF_1 (%)	96	96	93	85	58
	NF_1 (%)	96	96	93	85	54
Array 128	PF_1 (%)	72	72	71	69	49
	NF_1 (%)	73	67	74	65	47
Array 64	PF_1 (%)	71	65	64	52	47
	NF_1 (%)	71	70	62	51	43
Array 8	PF_1 (%)	57	54	50	50	43
	NF_1 (%)	48	47	51	51	42

C. LIS aperture comparisons

In this case LIS with different apertures instead of linear arrays have been evaluated. Once again, the spacing is fixed to $\lambda/2$. The results are shown in Fig. 7 and summarized in Table IV.

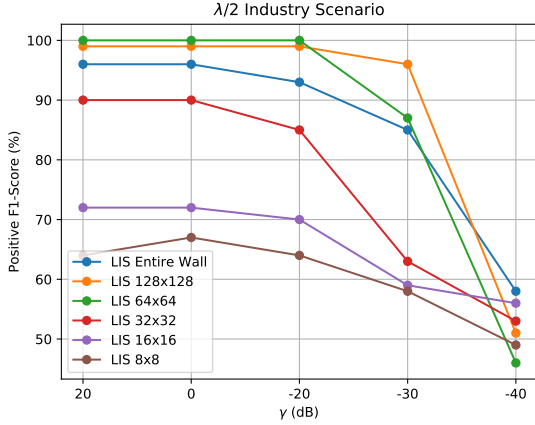


Fig. 7. Different LISs apertures comparison

Looking at Fig. 7, we can see a counterintuitive behavior at a first glance. Focusing for instance in the interval $\gamma \in [-20 \text{ dB}, 20 \text{ dB}]$, it is observed that the performance of the 64x64 and 128x128 LIS is higher than the LIS whose aperture is the entire wall. This interesting behavior may be related to the SNR distribution at each of the antenna elements. According to Section V-B, the noise samples added at each element are equally distributed, and their power is calculated with respect to the average SNR in both time and space. However, as the LIS dimensions become larger, the differences in the average received power at each antenna become non-negligible. Hence, the antennas variance of the SNR per element should increase with the LIS aperture, making that, although in practise we are increasing the number of elements to improve the image resolution, due to the presence of these low SNR at the edges, we may be actually losing information instead of taking advantage of the aperture increment.

TABLE IV. RESULTS SUMMARY LISS APERTURES COMPARISON

		γ				
		20	0	-20	-30	-40
LIS Entire Wall	PF_1	96	96	93	85	58
	NF_1	96	96	93	85	54
LIS 128x128	PF_1	99	99	99	96	51
	NF_1	99	99	99	96	53
LIS 64x64	PF_1	100	100	100	87	46
	NF_1	100	100	100	86	52
LIS 32x32	PF_1	90	90	85	63	53
	NF_1	91	91	87	60	49
LIS 16x16	PF_1	72	72	70	59	56
	NF_1	67	65	67	58	54
LIS 8x8	PF_1	64	67	64	58	49
	NF_1	59	62	59	51	47

VII. CONCLUSIONS

We have shown the potential of LIS for sensing the environment, being able to provide high resolution radio images of the propagation environment that can be processed by existing and versatile solutions in the context of computer vision algorithms. This sensing technique, which we consider appropriate to refer to as holographic sensing, arises as a robust solution to capture the large scale events of a target scenario, with the inherent advantage that the received signal phase does not need to be estimated. The combined used of both LIS and machine learning algorithms may be potentially used in the context of cognitive radio and multiuser massive MIMO as a support technology to enhance the performance of these systems.

REFERENCES

- [1] J. G. Andrews, S. Buzzi, W. Choi, S. V. Hanly, A. Lozano, A. C. Soong, and J. C. Zhang, "What will 5g be?" *IEEE J. Sel. Areas Commun.*, vol. 32, no. 6, pp. 1065–1082, 2014.
- [2] S. Hu, F. Rusek, and O. Edfors, "Beyond massive MIMO: The potential of data transmission with large intelligent surfaces," *IEEE Trans. Signal Process.*, vol. 66, no. 10, pp. 2746–2758, 2018.
- [3] E. Basar, "Transmission through large intelligent surfaces: A new frontier in wireless communications," in *EuCNC: Eur. Conf. Netw. Commun.* IEEE, 2019, pp. 112–117.
- [4] M.-A. Badiu and J. P. Coon, "Communication through a large reflecting surface with phase errors," *IEEE Wireless Commun. Lett.*, 2019.
- [5] E. Basar, M. Di Renzo, J. De Rosny, M. Debbah, M.-S. Alouini, and R. Zhang, "Wireless communications through reconfigurable intelligent surfaces," *IEEE Access*, vol. 7, pp. 116753–116773, 2019.
- [6] H. Wang, D. Zhang, Y. Wang, J. Ma, Y. Wang, and S. Li, "Rt-fall: A real-time and contactless fall detection system with commodity WiFi devices," *IEEE Trans. Mobile Comput.*, vol. 16, no. 2, pp. 511–526, 2016.
- [7] Q. Pu, S. Gupta, S. Gollakota, and S. Patel, "Whole-home gesture recognition using wireless signals," in *Proc. 19th Annual Inter. Conf. Mobile Comput. & Netw.*, 2013, pp. 27–38.
- [8] Y. Zhao, N. Patwari, J. M. Phillips, and S. Venkatasubramanian, "Radio tomographic imaging and tracking of stationary and moving people via kernel distance," in *2013 ACM/IEEE Inter. Conf. Inf. Process. Sensor Networks (IPSN)*. IEEE, 2013, pp. 229–240.
- [9] J. Wilson and N. Patwari, "Radio tomographic imaging with wireless networks," *IEEE Trans. Mobile Comput.*, vol. 9, no. 5, pp. 621–632, 2010.
- [10] M. Zhao, T. Li, M. Abu Alsheikh, Y. Tian, H. Zhao, A. Torralba, and D. Katabi, "Through-wall human pose estimation using radio signals," in *Proc. IEEE Conf. Comput. Vis. Pattern Recognit.*, 2018, pp. 7356–7365.
- [11] F. Adib, Z. Kabelac, H. Mao, D. Katabi, and R. C. Miller, "Real-time breath monitoring using wireless signals," in *Proc. 20th Annual Inter. Conf. Mobile Comput. Netw.*, 2014, pp. 261–262.
- [12] J. Joung, "Machine learning-based antenna selection in wireless communications," *IEEE Commun. Lett.*, vol. 20, no. 11, pp. 2241–2244, 2016.
- [13] O. T. Demir and E. Bjornson, "Channel estimation in massive MIMO under hardware non-linearities: Bayesian methods versus deep learning," *IEEE O. J. Commun. Soc.*, vol. 1, pp. 109–124, 2020.
- [14] R. Syms, "Practical volume holography clarendon," *Oxford*, vol. 19902, p. 125, 1990.
- [15] S. J. Pan and Q. Yang, "A survey on transfer learning," *IEEE Trans. Knowl. Data Eng.*, vol. 22, no. 10, pp. 1345–1359, 2009.
- [16] D. Sarkar, R. Bali, and T. Ghosh, *Hands-On Transfer Learning with Python: Implement advanced deep learning and neural network models using TensorFlow and Keras*. Packt Publishing Ltd, 2018.
- [17] F. Chollet *et al.*, "Keras," <https://keras.io>, 2015.
- [18] C. M. Bishop, *Pattern recognition and machine learning*. Springer, 2006.

- [19] Winprop, altair engineering, inc. <https://www.altairhyperworks.com/winprop>.
- [20] D. Anguita, A. Ghio, S. Ridella, and D. Sterpi, "K-fold cross validation for error rate estimate in support vector machines." in *DMIN*, 2009, pp. 291–297.
- [21] D. M. Powers, "Recall & precision versus the bookmaker." International Conference on Cognitive Science, 2003.